Journal of Materials Chemistry

Cite this: J. Mater. Chem., 2012, 22, 15357

www.rsc.org/materials

PAPER

Optimizing Li^+ conductivity in a garnet framework

Yutao Li,[ab] Jian- Tao Han,[b] Chang- An Wang,[a] Hui Xie[b] and John B. Goodenough*[b]

Received 7th March 2012, Accepted 3rd June 2012
DOI: 10.1039/c2jm31413d

The garnet-related oxides with the general formula $Li_{7-x}La_3Zr_{2-x}Ta_xO_{12}$ ($0 \le x \le 1$) were prepared by conventional solid-state reaction. X-ray diffraction (XRD), neutron diffraction and AC impedance were used to determine phase formation and the lithium-ion conductivity. The lattice parameter of $Li_{7-x}La_3Zr_{2-x}Ta_xO_{12}$ decreased linearly with increasing x. Optimum Li-ion conductivity in the Li-ion garnets $Li_{7-x}La_3Zr_{2-x}Ta_xO_{12}$ is found in the range $0.4 \le x \le 0.6$ for samples fired at 1140 °C in an alumina crucible. A room-temperature $\sigma_{Li} \approx 1.0 \times 10^{-3}$ S cm^{-1} for $x = 0.6$ with an activation energy of 0.35 eV in the temperature range of 298–430 K makes this Li-ion solid electrolyte attractive for a new family of Li-ion rechargeable batteries.

Introduction

Integration of alternative energy technologies into the grid depends on the availability of adequate electrical-energy storage. The most important challenge for further development of Li-ion batteries for this application is increased capacity. Limitations of the flammable organic liquid-carbonate electrolytes of the Li-ion battery have stimulated interest in Li-ion solid electrolytes having a $\sigma_{Li} > 10^{-3}$ S cm^{-1} at room temperature that are stable on contact with a lithium anode on one side and with water of variable pH or an alternative liquid on the other side.[1] If the electrolyte is to separate a lithium anode and an air or liquid cathode, the solid electrolyte must be an oxide; such a solid oxide electrolyte would allow development of Li-ion batteries of higher storage capacity by allowing cathodes other than the present Li-insertion compounds as well as lithium anodes.[2]

Garnet-related Li-rich metal oxides have been studied extensively since the observation of a Li-ion conductivity $\sigma_{Li} > 10^{-4}$ S cm^{-1} at 25 °C in $Li_7La_3Zr_2O_{12}$,[3] which is stable on contact with a lithium anode. A variety of compositional variations have been investigated, including $Li_5La_3M_2O_{12}$ (M = Nb, Ta, Sb, Bi)[4–6] and $Li_6ALa_3M_2O_{12}$ (A = Ca, Sr, Ba; M = Nb, Ta)[7,8] in order to vary the lattice constant and Li-ion population. Kotobuki *et al.*[8a] have shown that addition of Al_2O_3 helps sintering of $Li_7La_3Zr_2O_{12}$ without hindering the Li^+ framework. The highest $\sigma_{Li} = 8 \times 10^{-4}$ S cm^{-1} was obtained in the "$Li_{6.75}La_3Zr_{1.75}Nb_{0.25}O_{12}$" garnet by Shingo Ohta *et al.*[9]

The garnet structure $A_3B_3C_2O_{12}$ contains a $B_3C_2O_{12}$ framework structure of B cations in 8-coordination sites and C cations in octahedral sites. The framework contains a 3D-connected interstitial space consisting of the tetrahedral 24*d*-A sites bridged by a single octahedron sharing on opposite sides a common face with each of the two neighboring A sites. The bridging octahedral sites share common edges. The existence of 3 tetrahedral-A and 6 bridging-octahedral sites for a total of 9 sites per formula unit can provide a low activation energy for motion of guest lithium ions if the lithium ions are disordered with a partial occupancy of both sites.

In previous work, we studied by neutron-diffraction a cubic aluminum-free $Li_7La_3Zr_2O_{12}$ sample prepared at 750 °C;[10] we deduced that since coulomb repulsions prevent occupancy of an octahedral site with two near-neighbor tetrahedral sites occupied, $x = 7.5$ is the upper limit of x that can be tolerated in a $Li_xB_3C_2O_{12}$ garnet framework and that this ideal limit requires 1.5 per formula unit of long-range-ordered vacancies in the tetrahedral 24*d* sites. We have found that Ta-doped $Li_6La_3ZrTaO_{12}$ (ref. 11) has shown high lithium conductivity $\sigma_{Li} > 10^{-4}$ S cm^{-1}. Doping with higher-valence cations increases the Li-ion vacancy concentration and significantly reduces the degree of local ordering. A $\sigma_{Li} \approx 1.0 \times 10^{-3}$ S cm^{-1} has been obtained by MD simulations in $Li_{6.75}La_3Zr_{1.75}Ta_{0.25}O_{12}$.[12] In order to determine the optimum concentration of Li-ions in the garnet framework, we have undertaken a study of nominal $Li_{7-x}La_3Zr_{2-x}Ta_xO_{12}$; Ta(v) was chosen as the dopant as, like Zr(IV), it is not reduced on contact with lithium. Here we report a solid oxide Li-ion electrolyte having a Li-ion conductivity $\sigma_{Li} \approx 1.0 \times 10^{-3}$ S cm^{-1} at room temperature.

Methods

Compounds with the nominal chemical formula $Li_{7-x}La_3Zr_{2-x}Ta_xO_{12}$ were prepared by solid-state reaction of stoichiometric amounts of Li_2CO_3, La_2O_3 (heated at 900 °C for 12 h), ZrO_2 and Ta_2O_5. 10 wt% excess Li_2CO_3 was added to compensate for the loss of lithium during annealing. The

[a]State Key Laboratory of New Ceramics and Fine Processing, Department of Materials Science and Engineering, Tsinghua University, Beijing 100084, P.R. China
[b]Materials research program and the Texas Materials Institute, ETC9.184, University of Texas at Austin, Texas 78712, USA. E-mail: jgoodenough@mail.utexas.edu

powders were ground and heated to 900 °C to decompose the metal salts. Finally, the powders were ground again, pressed into a pellet, and annealed at 1120 °C for 8 h ($x = 1$ and 0.8), 1140 °C for 16 h ($x = 0.6$, 0.4, and 0.2), at 1230 °C for 36 h ($x = 0$) in air while the pellet was covered with the same mother powder. The annealing was done in an alumina crucible.

Powder X-ray diffraction (Philips PW1830, Cu Kα) was employed to monitor the phase formation in the 2θ range from 10 to 70° with a step size of 0.02°. The lattice parameters were calculated from the diffraction peaks in the range 20–60° with Jade software. A field-emission scanning electron microscope (Quanta FEG650) was used to obtain the fracture surface microstructure of the pellet. The composition distribution of the elements was measured by inductively coupled plasma optical emission spectroscopy (ICP-OES) and energy dispersive spectroscopy.

Neutron diffraction experiments were conducted with the high-pressure preferred-orientation neutron diffractometer (HIPPO) at the Lujan Neutron Scattering Center, Los Alamos National Laboratory. Bulk samples were placed in a vanadium holder and time-of-flight data were collected under vacuum at room temperature. Neutrons were detected with 27 detector panels of ^{3}He detector tubes arranged on three rings with nominal diffraction angles of 40°, 90°, and 144°. The GSAS program was used to perform Rietveld refinement with background functions type 1 and 20 for background coefficients.

Ionic conductivity was measured from 298 to 430 K with a Solartron Impedance Analyzer (Model 1260); the applied frequency range was from 10^6 to 1 Hz with an AC amplitude of 10 mV. Both parallel surfaces of the pellet were sputtered with Li-ion-blocking Au electrodes. The electronic resistivity measurement at room temperature was performed with a four-probe technique on specimens with a rectangular geometry (2 mm × 2 mm × 1 mm).

The electrochemical windows of the samples were evaluated by cyclic voltammetry (CV) with a Solartron Impedance Analyzer (Model 1260) at a scanning rate of 1 mV s^{-1} between −0.5 and 5 V (*vs.* Li$^+$/Li). A gold electrode and lithium metal were attached to opposite faces of the pellet as working electrodes and counter electrodes; the cell was fabricated in a glove box under Ar atmosphere.

Results and discussion

Fig. 1(a) shows the powder XRD patterns for different compositions sintered in an alumina crucible; the diffraction peaks observed after heat treatment were assigned to a well-crystallized garnet-related structure. All the garnet frameworks crystallize in the space group $Ia\bar{3}d$. The lattice parameter of $Li_{7-x}La_3Zr_{2-x}Ta_xO_{12}$ decreased nearly linearly with increasing x according to Végard's law as shown in Fig. 1(b). The lattice parameters are influenced somewhat by different Li$^+$ and Al^{3+} distributions in the interstitial space.

For $x = 0.6$, ICP confirmed the presence of 2.5 wt% Al^{3+} originating from the alumina crucible. The molar ratio of the elements Li$^+$: Al^{3+} : La^{3+} was 6.32 : 0.08 : 2.91. In addition, we have shown with electron-energy dispersive spectroscopy that most (Fig. 2(b)), if not all, of the Al^{3+} entering a polycrystalline sample from the alumina crucible is located in the grain boundaries for $x = 0.6$. The Li_2O-doped Al_2O_3 in the grain boundaries acts as a sintering aid, provides Li-ion conductivity across the grain boundaries, and suppresses excess Li loss from the sample at sintering temperatures above 850 °C. Good connection between the powders after sintering (as seen in Fig. 2(a)) can reduce the intergrain ionic resistance as well.

In order to identify the Li-ion distribution inside the garnet grains, neutron diffraction was introduced to confirm the structures of $^7Li_{6.5}La_3Zr_{1.5}Ta_{0.5}O_{12}$ and $^7Li_7La_3Zr_2O_{12}$ powders. O'Callaghan and Cussen[13,14] have used neutron diffraction to follow the site occupancies with increasing x; they report that the occupancy of the tetrahedral A sites 24*d* decreases monotonically with x in the range $5 \leq x < 6.6$ with an associated increase with x in the 96*h* sites. These data indicate that the Li-ions have a site preference for the 24*d* site, and the octahedral 48*g* lithium ions are displaced to the 96*h* site by Li$^+$ occupancy of one neighboring 24*d* site. Their data also indicate the possible onset of short-range ordering of 24*d*-site vacancies for $x > 6.4$. Since regions of short-range order would inhibit Li-ion mobility, we had particular interest in the evolution of σ_{Li} with x of nominal $Li_{7-x}La_3Zr_{2-x}Ta_xO_{12}$ in the interval $0.4 < x < 0.8$.

The structure of cubic $Li_6BaLa_2Ta_2O_{12}$, in which the lithium was disordered with occupancies of 22% octahedral sites (48*g*), 21.8% displaced in octahedral sites (96*h*), and 67.4% tetrahedral sites (24*d*), was adopted as the initial structure model for all garnet materials here. The lattice parameters, atomic positions and occupancies, isotropic displacement parameters, and peak widths in the profile function were all refined. With these refinement conditions, the reliability factors converged to satisfactory values. The details of the data collection and a fitted diffraction pattern "$^7Li_{6.5}La_3Zr_{1.5}Ta_{0.5}O_{12}$" and "$^7Li_7La_3Zr_2O_{12}$" are shown in Tables 1 and 2 and in Fig. 3.

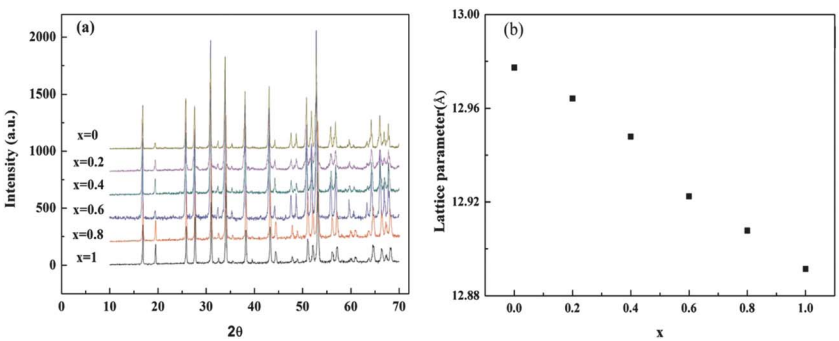

Fig. 1 (a) Powder XRD result of $Li_{7-x}La_3Zr_{2-x}Ta_xO_{12}$. (b) Lattice parameter of $Li_{7-x}La_3Zr_{2-x}Ta_xO_{12}$.

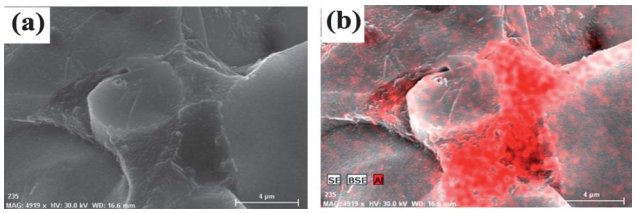

Fig. 2 (a) Scanning electron micrograph and (b) Al distribution (pink) in a nominal $Li_{6.4}La_3Zr_{1.6}Ta_{0.6}O_{12}$ sample.

Table 1 Structural parameters of "$^7Li_7La_3Zr_2O_{12}$" garnet from Rietveld refinement of neutron diffraction data

Atom	Site	*x*, *y*, *z*	Occupation	U_{iso}
Li1	24*d*	0.375, 0, 0.25	0.363(1)	0.033(4)
Li2	48*g*	0.125, 0.6796(7), 0.5704(7)	0.250(2)	0.00149(7)
Li3	96*h*	0.0912(7), 0.19415(6), 0.4237(4)	0.350(1)	0.0201(23)
La	24*c*	0.125, 0, 0.25	1	0.00724(15)
Zr	16*a*	0, 0, 0	1	0.00716(22)
O	96*h*	0.0999(4) 0.1958(9) 0.281(8)	0.99(3)	0.01070(19)
R_p/R_{wp}/ CHI^2	0.0097/0.0075/ 10.19			

Table 2 Structural parameters of "$^7Li_{6.5}La_3Zr_{1.5}Ta_{0.5}O_{12}$" garnet from Rietveld refinement of neutron diffraction data

Atom	Site	*x*, *y*, *z*	Occupation	U_{iso}
Li1	24*d*	0.375, 0, 0.25	0.388(8)	0.0132(14)
Li2	48*g*	0.125, 0.6835(8), 0.5664(2)	0.288(7)	0.0082(14)
Li3	96*h*	0.0929(6), 0.1927(8), 0.4241(7)	0.247(1)	0.0131(16)
La	24*c*	0.125, 0, 0.25	1	0.00767(20)
Zr	16*a*	0, 0, 0	0.75	0.0095(23)
Ta	16*a*	0, 0, 0	0.25	0.0095(23)
O	96*h*	0.1015(9), 0.1975(6) 0.2807(2)	0.99(5)	0.0100(2)
R_p/R_{wp}/ CHI^2	0.0071/0.0053/ 9.570			

In space group $Ia\bar{3}d$, the Zr(Ta) and La ions of the La_3Zr-TaO_{12} garnet framework occupy, respectively, octahedral 16*a* and 8-coordinated 24*c* sites. Our cubic garnet "$^7Li_{6.5}La_3Zr_{1.5}Ta_{0.5}O_{12}$" and "$^7Li_7La_3Zr_2O_{12}$" had space group $Ia\bar{3}d$ with lattice parameter $a = 12.9450$ and 12.9720 Å at room temperature; 5.85 and 6.79 lithium ions per formula unit, respectively, were located at three different positions (48*g*, 96*h*, and 24*d*). The Li-ions occupying the three different positions form a continuous 3D network of moving Li^+ ions in the interstitial space of the 3D garnet framework. The four-coordinated 24*d* Li sites and displaced 96*h* sites show a significantly larger displacement parameter than that of the octahedral 48*g* Li sites.

In $Li_xB_3C_2O_{12}$, the cubic garnet phase is difficult to obtain for $x > 7.0$, and $x = 7.5$ is the upper limit of x that can be tolerated in a $Li_xB_3C_2O_{12}$ garnet framework; more Li^+ can lead to short Li^+–Li^+ distances that destabilize the garnet framework. For $x = 3$, $Li_3Ln_3Te_2O_{12}$ (Ln = rare earth)[15] with Li^+ ions only in the tetrahedral sites shows lower Li^+ conductivity by 2–3 orders of magnitude compared to $Li_7La_3Zr_2O_{12}$, while the Li^+ conductivity in $Li_6La_3ZrTaO_{12}$ is comparable to that in $Li_7La_3Zr_2O_{12}$, which indicates that the Li^+ conductivity may be optimized in the interval $6 < x < 7$. In both as synthesized $x = 0.5$ and $x = 0$ samples, the lithium ions occupy about 36% tetrahedral sites. With the Li population increase to $x = 0$, the octahedral lithium ions force more Li off the tetrahedral sites; 38.8% Li occupancy of the tetrahedral site in "$^7Li_{6.5}La_3Zr_{1.5}Ta_{0.5}O_{12}$" is reduced to 36.3% in the "$^7Li_7La_3Zr_2O_{12}$" and 24.7% Li occupancy of the displaced octahedral 96*h* site is increased to 35.0% in the "$^7Li_7La_3Zr_2O_{12}$", which is consistent with extrapolation of O'Callaghan and Cussen's data.[13] The tetrahedral sites (24*d*) were 67.4%, 38.8% and 36.3% occupied, while the octahedral sites (48*g* and 96*h*) were 65.6%, 78.2% and 95% occupied and the Li^+ conductivity was 4×10^{-5}, 9.2×10^{-4} and 1.4×10^{-4} S cm^{-1}, respectively, for $x = 6$ (ref. 8 and 13), 6.5 and 7 in $Li_xB_3C_2O_{12}$. The Li^+ conductivity in $Li_{7-x}La_3Zr_{2-x}Ta_xO_{12}$ increased with x and reached a maximum around $x = 0.4$. The high Li^+ conductivity in $Li_{7-x}La_3Zr_{2-x}Ta_xO_{12}$ indicates that the appropriate Li^+ concentration for Li^+ transport is in the range $6.4 \leq x \leq 6.6$ in $Li_xB_3C_2O_{12}$. Some Li^+ vacancies in the octahedral sites improve the Li^+ conductivity significantly, and the best ratio of Li^+ occupancy/vacancy of the octahedral sites appears to be around 3 : 1.

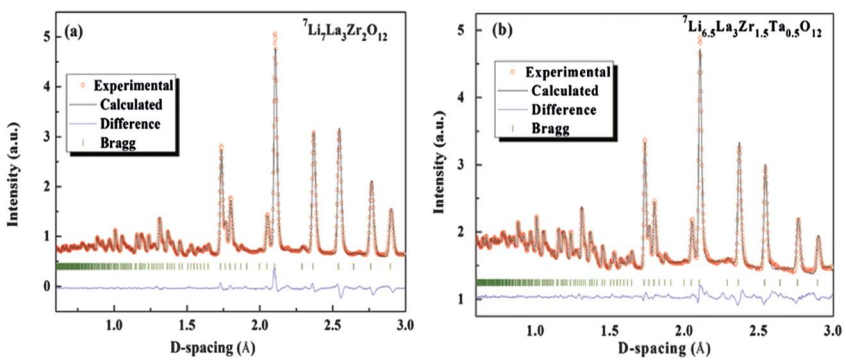

Fig. 3 Observed, calculated, and difference patterns for the Rietveld refinement from neutron diffraction of garnet before ion exchange. The short vertical lines below the profiles mark the peak positions of all possible Bragg reflections.

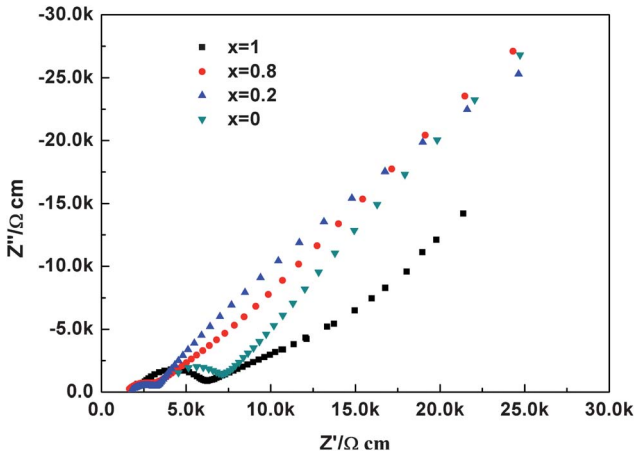

Fig. 4 Impedance plot (1–10^6 Hz) of $Li_{7-x}La_3Zr_{2-x}Ta_xO_{12}$ measured in air at 25 °C.

The lithium ions occupy the 24*d* tetrahedral and distorted octahedral sites. The short Li^+–Li^+ contact (1.987 Å for $x = 0$ and 1.986 Å for $x = 0.5$) between Li^+ in neighboring 24*d* and 48*g* sites introduces a Coulomb repulsion that displaces the lithium ions in the octahedral site to a 96*h* site neighboring an empty 24*d* site to give a Li^+–Li^+ separation (2.433 Å for $x = 0$ and 2.438 Å for $x = 0.5$); a lithium ion is not stable in a 48*g* site that bridges two occupied 24*d* sites.

Fig. 4 displays typical room-temperature impedance plots measured in air for $x = 0$, 0.2, 0.8 and 1. The linear low-frequency portion signals that the conductivity is primarily ionic. Only one clear semicircle was observed in the high-frequency region, and the distance from zero to the intercept of the linear tail with the real axis was assigned to the total conductivity. The bulk and grain-boundary resistance could be obtained by fitting the experimental data with the conventional equivalent circuit consisting of $(R_b)(R_{gb}CPE1)(CPE2)$. The total ionic conductivities of "$Li_{7-x}La_3Zr_{2-x}Ta_xO_{12}$" for $x = 0$, 0.2, 0.8 and 1 were 1.2×10^{-4}, 2.8×10^{-4}, 3.2×10^{-4} and 1.6×10^{-4} S cm^{-1}. Fig. 5(a) displays typical room-temperature impedance plots measured in air for $0.4 \leq x \leq 0.6$. The total ionic conductivities of "$Li_{7-x}La_3Zr_{2-x}Ta_xO_{12}$" with $x = 0.4$, 0.5 and $x = 0.6$ at 25 °C were 7.3×10^{-4}, 9.2×10^{-4} and 1.0×10^{-3} S cm^{-1}, respectively. Since the samples had a tan color, suggestive of color centers at oxygen vacancies, a four-point system was used to determine the electronic conductivity. For the sample with $x = 0.6$ (2 mm × 2 mm × 1 mm), the electronic resistance was not measurable, which indicates that the garnet electrolyte here is a good electronic insulator.

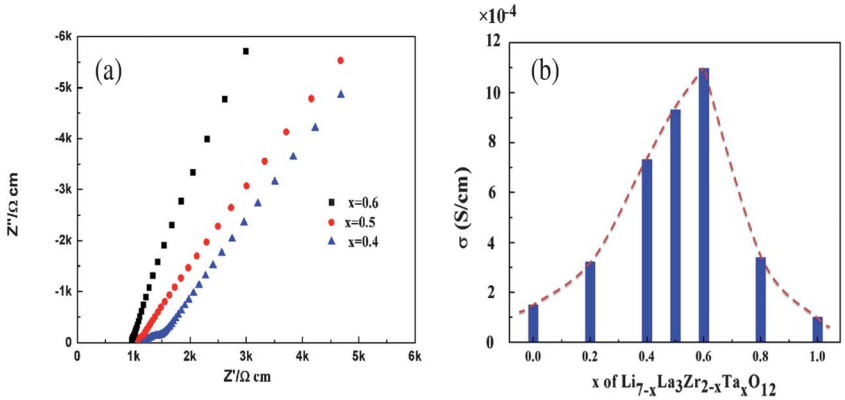

Fig. 5 (a) Impedance plot (1–10^6 Hz) of $Li_{7-x}La_3Zr_{2-x}Ta_xO_{12}$ measured in air at 25 °C. (b) Lithium conductivity change with *x*.

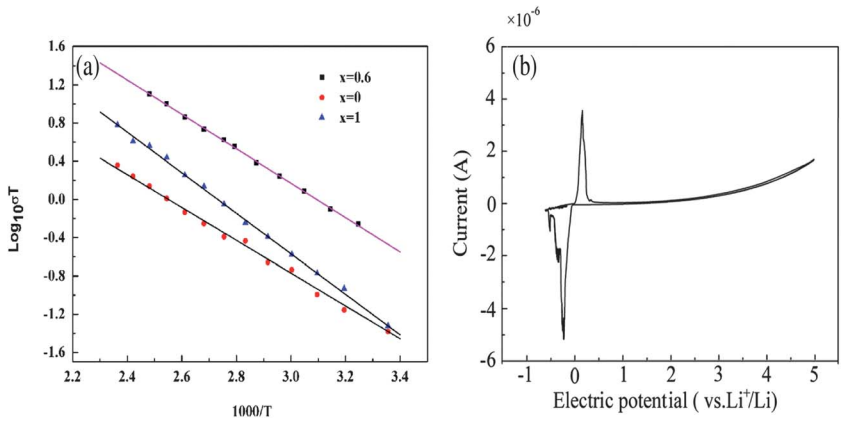

Fig. 6 (a) Arrhenius plot of ionic conductivity of $Li_{6.4}La_3Zr_{1.4}Ta_{0.6}O_{12}$. (b) A cyclic voltammogram of $Li_{6.4}La_3Zr_{1.4}Ta_{0.6}O_{12}$ electrolyte at a scanning rate of 1 mV s^{-1} at 25 °C.

Fig. 5(b) shows the variation with x of the room temperature σ_{Li} for $0 \leq x \leq 1$ of $Li_{7-x}La_3Zr_{2-x}Ta_xO_{12}$; a maximum $\sigma_{Li} \approx 1.0 \times 10^{-3}$ S cm^{-1} was found for $x = 0.6$. Fig. 6(a) shows the Li-ion conductivity as a function of $1000/T$ for a sintered sample of "$Li_{7-x}La_3Zr_{2-x}Ta_xO_{12}$" ($x = 0$, 0.6 and 1).

The temperature dependence of the conductivity can be expressed by the Arrhenius equation.

$$\sigma T = A\exp(-E_a/kT)$$

The activation energy of "$Li_{7-x}La_3Zr_{2-x}Ta_xO_{12}$" with $x = 0.6$ was estimated to be $E_a = 0.35$ eV from the slope of the log σT *versus* $1000/T$ plot in the temperature range of 298–430 K. A cyclic voltammogram of $Li_{6.4}La_3Zr_{1.6}Ta_{0.6}O_{12}$ is shown in Fig. 6(b), which reveals lithium deposition and dissolution peaks near 0 V *vs.* Li^+/Li; there is no other reaction up to 5 V *vs.* Li^+/Li, indicating that the electrolyte here is stable with lithium metal.

Conclusion

The garnet-related oxide with the general formula $Li_{7-x}La_3Zr_{2-x}Ta_xO_{12}$ ($0 \leq x \leq 1$) prepared by conventional solid-state reaction is cubic and crystallizes in the space group $Ia\bar{3}d$. The lattice parameter of $Li_{7-x}La_3Zr_{2-x}Ta_xO_{12}$ decreased linearly with increasing x. The optimum Li-ion conductivity in the Li-ion garnets $Li_{7-x}La_3Zr_{2-x}Ta_xO_{12}$ is found in the range $0.4 \leq x \leq 0.6$ for samples fired at 1140 °C in an alumina crucible. A room-temperature $\sigma_{Li} \approx 1.0 \times 10^{-3}$ S cm^{-1} for $x = 0.6$ makes this Li-ion solid electrolyte attractive for a new family of Li-ion rechargeable batteries. Although the oxide is reported to be unstable in an aqueous electrolyte,[16] this problem can be solved. Moreover, the electrolyte may be stable in alternative liquid cathodes. The adventitious Al of the $x = 0.6$ composition appears to reside primarily in an amorphous grain-boundary phase where it acts as a sintering aid and blocks excessive Li loss at the sintering temperature.

Acknowledgements

Yutao Li thanks the China Scholarship Council for the opportunity to work in Texas. This work was supported by the Assistant Secretary for Energy Efficiency and Renewable Energy, Office of Vehicle Technologies, U.S. Department of Energy, under Contract DE-AC02-05CH11231 through the Batteries for Advanced Transportation Technologies (BATT) Program Subcontract 6805919. The work was also supported by the Office of Basic Energy Sciences, Office of Science, U.S. Department of Energy, under Contract DESC0005397. The Robert A. Welch Foundation of Houston Tx, is also thanked for financial support.

References

1 J. B. Goodenough and Y. Kim, *Chem. Mater.*, 2010, **22**, 587–603.
2 Y. Lu, J. B. Goodenough and Y. Kim, *J. Am. Chem. Soc.*, 2011, **133**, 5756–5759.
3 R. Murugan, V. Thangadurai and W. Weppner, *Angew. Chem., Int. Ed.*, 2007, **46**, 7778–7781.
4 V. Thangadurai, H. Kaack and W. J. F. Weppner, *J. Am. Ceram. Soc.*, 2003, **86**, 437–440.
5 R. Murugan, W. Weppner, P. Schmid-Beurmann and V. Thangadurai, *Mater. Sci. Eng., B*, 2007, **143**, 14–20.
6 R. Murugan, W. Weppner, P. Schmid-Beurmann and V. Thangadurai, *Mater. Res. Bull.*, 2008, **43**, 2579–2591.
7 R. Murugan, V. Thangadurai and W. Weppner, *Ionics*, 2007, **13**, 195–203.
8 V. Thangadurai and W. Weppner, *Adv. Funct. Mater.*, 2005, **15**, 107–112; M. Kotobuki, K. Kanamura, Y. Sato and T. Yoshida, *J. Power Sources*, 2011, **196**, 7750–7754.
9 S. Ohta and T. Kobayashi, *et al.*, *J. Power Sources*, 2011, **196**(6), 3342–3345.
10 H. Xie, *et al.*, *Chem. Mater.*, 2011, **23**(16), 3587–3589.
11 Y. Li, *et al.*, *Electrochem. Commun.*, 2011, **13**(12), 1289–1292.
12 S. Adams and R. P. Rao, *J. Mater. Chem.*, 2012, **22**, 1426–1434.
13 M. P. O'Callaghan and E. J. Cussen, *Chem. Commun.*, 2007, 2048–2050.
14 E. J. Cussen, *Chem. Commun.*, 2006, 412–413.
15 M. P. O'Callaghan, D. R. Lynham, G. Z. Chen and E. J. Cussen, *Chem. Mater.*, 2006, **18**, 4681–4689.
16 C. Galven and J.-L. Fourquet, *et al.*, *Chem. Mater.*, 2011, **23**(7), 1892–1900.